25th ABCM International Congress of Mechanical Engineering
October 20-25, 2019, Uberlândia, MG, Brazil

COBEM2019-0966
VIBRATION RESPONSES OF A CRACKED ROTATING SHAFT WITH COMBINATION RESONANCES TECHNIQUE

Izabela Batista da Silva
Aldemir Ap Cavalini Jr.
Valder Steffen Jr.
LMEst - Structural Mechanics Laboratory, Federal University of Uberlândia, School of Mechanical Engineering, Av. João Naves de Ávila, 2121, Uberlândia, MG, 38408-196, Brazil
izabela.silva@ufu.br, aacjunior@ufu.br, vsteffen@ufu.br

Abstract. *Recently, a crack identification methodology based on parametric vibration responses was proposed. This technique uses externally applied forces at specific frequencies attaining combination resonances to characterize crack signatures in the spectral responses of flexible rotors. The multiple scale method is used to determine the conditions required to create resonances on the system as a combination of the excitation frequency and the critical speeds of the machine. The external force is applied in the shaft operating under a steady-state condition. In this context, the present work compares the numerical and experimental vibration responses of a horizontal rotating shaft with a breathing crack. The combination resonances on the spectral vibration responses of the rotor are verified in both numerical and experimental tests. Similar results were obtained.*

Keywords: *rotating machines, transverse cracks, combination resonances, breathing behavior.*

1. INTRODUCTION

Nonlinear dynamic systems can be found in several fields of engineering and require complex methods for modeling and predicting their behavior. Regarding mechanical engineering problems, rotating systems with flexible shafts in the presence of faults may show a pronounced nonlinear behavior.

Ishida and Yamamoto (2013) give some examples of failures that produce nonlinear effects in rotating machines, such as clearance in ball bearings, oil film in a journal bearing, clearance in a squeeze-film damper bearing, and transverse cracks in shafts. In the case of transverse cracks, Gasch (1976), Mayes and Davies (1984), and Bachschmid *et al.* (2010) proposed different formulations aiming at modeling the associated nonlinear behavior. These models describe the breathing mechanism, the phenomena for opening and closing the crack according to angular shaft position. Many researchers investigated the influence of cracks in shafts of rotating machines aiming to predict, detect, and indicate their position Grabowski (1980); Saavedra and Cuitino (2002); Sinou and Lees (2005); Zhao *et al.* (2014); Lu *et al.* (2017).

Periodic external excitation can be used to highlight the nonlinear effects of cracks present in rotating shafts. Additional frequencies are verified in the spectral responses of the system when the external force is applied (Sawicki *et al.*, 2009). These frequencies are known as combination resonances, and can be used as indicators of crack presence. The appearance of combination resonances in a cracked shaft was first introduced by Iwatsubo *et al.* (1992). The authors proposed an SHM (Structural Health Monitoring) technique based on periodical external excitation for crack detection in rotating machines. However, the appearance of combination resonances is not efficient to indicate the location of the crack along the shaft. Thus, the methodology proposed by Iwatsubo *et al.* (1992) should be combined with other techniques. A crack identification methodology based on combination resonances was presented numerically by Cavalini Jr *et al.* (2016).

In this context, the present contribution aims at comparing numerical and experimental results on the appearance of combination resonances in the vibration responses of a rotating machine with a cracked shaft. In this case, the finite element (FE) model of a horizontal shaft is used. The breathing crack behavior is modeled according to the Mayes' model and the Linear Fracture Mechanics (Mayes and Davies, 1984).

2. ROTOR TEST-RIG

The rotor test-rig used in the present work is shown in Fig. 1, in which a crack with 50% depth is present in the mid-span of the shaft. The rotating machine is composed of a flexible steel shaft with 850 mm length and 19 mm diameter (E = 182 GPa, ρ = 7930 kg/m^3, and ν = 0.29), two rigid discs D_1 and D_2, both of aluminum with 150 mm diameter and 20 mm

thickness, and two self alignment ball bearings (B_1 and B_2). In this case, displacement measurements were performed along the horizontal direction of the shaft using a laser sensor connected to the signal analyzer Agilent (model 35670A). An electromechanical shaker was used to apply the external excitation horizontally in the right-hand-side bearing of the rotating machine. The force amplitude was measured using a dynamic load cell.

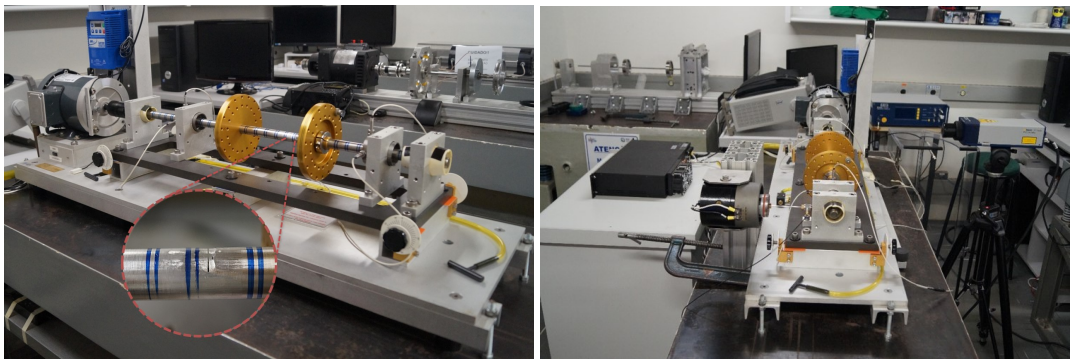

(a) Rotating machine with a 50% crack depth in the shaft. (b) Electromechanical shaker used to apply the external excitation

Figure 1. Rotor test rig.

3. ROTOR MODELING

The FE model used to represent the rotor test-rig was formulated based on the Timoshenko beam theory with 35 finite elements, as shown in Fig. 2. The considered shaft element has 2 nodes with 4 degrees of freedom each node; two lateral displacements and two rotations (u, w, θ, φ). The discs D_1 and D_2 are located at the nodes #18 and #25, respectively (rigid discs). The bearings B_1 and B_2 are located at the nodes #6 and #33, respectively. In this case, the vibration responses of the shaft are collected along the horizontal direction of the nodes #8 (S_{8X} and S_{8Z}) and #28 (S_{28X} and S_{28Z}). It is worth mentioning that the experimental measurements were performed along the corresponding positions of the rotating machine presented in Fig. 1.

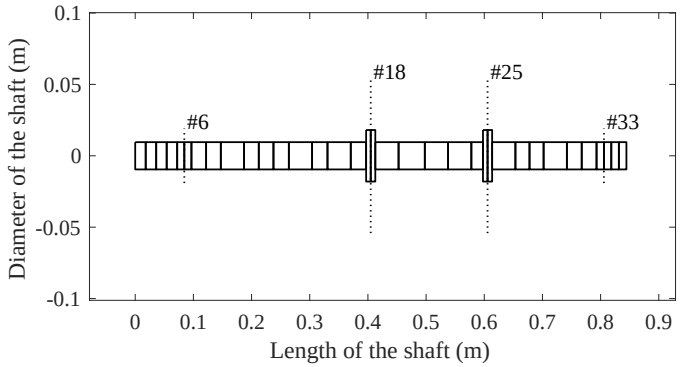

Figure 2. Shaft-bearing-disc FE model.

The dynamic behavior of the considered rotating machine (FE model) is mathematically represented as:

$$\mathbf{M}\ddot{\mathbf{q}} + [\mathbf{D} + \Omega\mathbf{D}_g]\,\dot{\mathbf{q}} + \mathbf{K}\,(\Omega t)\,\mathbf{q} = \mathbf{W} + \mathbf{F}_u + \mathbf{F}_{diag} \tag{1}$$

where $\mathbf{M}$ is the mass matrix, $\mathbf{D}$ is the damping matrix, $\mathbf{K}(\Omega t)$ is the stiffness matrix with variable values due to the crack existence (i.e., Ωt stands for the angular position of the shaft), Ω is the rotation speed of the shaft, t is the time, $\mathbf{W}$ stands for the weight of the rotating parts, $\mathbf{F}_u$ is the unbalance forces, $\mathbf{F}_{diag}$ is the diagnostic force applied in the rotor, and $\mathbf{q}$ is the generalized displacement vector.

A model updating procedure based on numerical and experimental FRFs (frequency response functions) was performed to obtain a representative FE model of the rotor. Thus, the stiffness and damping coefficients of the bearings, the proportional damping added to $\mathbf{D}$ (coefficients γ and β; $\mathbf{D}_p$=γM+βK), and the angular stiffness k_{ROT} due to the coupling between the electric motor and the shaft were determined solving a typical inverse problem. In this case, the heuristic optimization technique Differential Evolution (Storn and Price, 1995) was used. The considered objective function is

presented in Eq. (2).

$$DE_{OF} = \sum_{i=1}^{N} \sum_{j=1}^{n_p} \frac{\|FRF_{exp,i,j} - FRF_{num,i,j}\|}{\|FRF_{exp,i,j}\|} \tag{2}$$

where $FRF_{exp,i,j}$ and $FRF_{num,i,j}$ represent the experimental and numerical FRFs, N is the number of FRFs, and n_p is the number of frequency points evaluated in the FRFs.

Table 1 summarizes the results obtained using the model updating procedure.

Table 1. Parameters determined by using the model updating procedure.

Stiffnesses	Values	Damping	Values	Proportional damping	Values
$k_{X/B1}$ [N/m]	2.699x10^9	$d_{X/B1}$ [Ns/m]	87.331	γ	149.997
$k_{Z/B1}$ [N/m]	9.541x10^7	$d_{Z/B1}$ [Ns/m]	45.489	β	9.953x10^{-6}
$k_{X/B2}$ [N/m]	3.979x10^9	$d_{X/B2}$ [Ns/m]	26.915	-	-
$k_{Z/B2}$ [N/m]	8.935x10^7	$d_{Z/B2}$ [Ns/m]	125.849	-	-
k_{ROT} [N/rad]	3.377x10^3	-	-	-	-

For this configuration, the first and second forward whirl critical speeds of the rotating machine were 53.09 Hz and 207.81 Hz, respectively. The first and second backward whirl critical speeds were 51.85 Hz and 190.15 Hz, respectively.

3.1 Crack breathing model

The shaft FE model with crack was obtained using first the linear fracture mechanics theory to determine the additional flexibility due to the crack existence. The model proposed by Mayes and Davies (1984) was adopted to represent the breathing behavior of the crack, i.e., the mechanism for opening and closing the crack. In this case, a cosine function is used to describe the breathing behavior. However, the Mayes' model is not able to correlate the additional flexibility of a shaft with the crack depth. Thus, the linear fracture mechanics theory must be applied.

In this formulation, it is assumed a beam element containing a transverse crack with depth α, as shown in Fig. 3

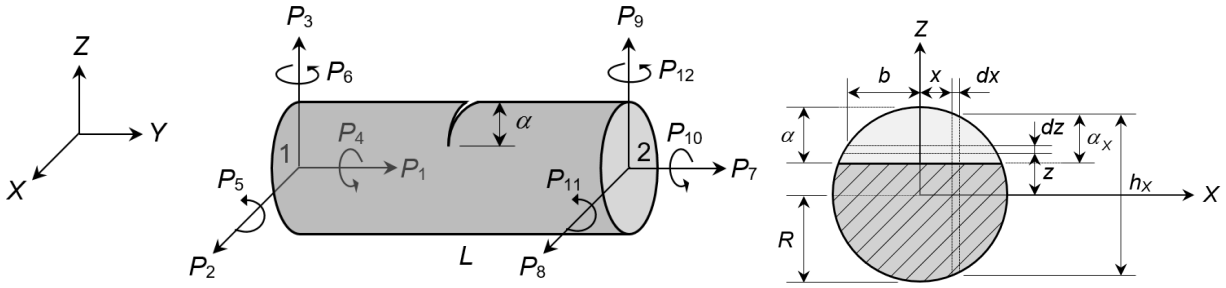

Figure 3. Shaft element with a crack.

The Castiglione theorem is used to determine the displacement of the shaft with a crack q_i in the direction of the applied load P_i Darpe *et al.* (2004), as presented by Eq. (3).

$$q_i = \frac{dU}{dP_i} = \frac{\partial U^0}{\partial P_i} + \frac{\partial U^c}{\partial P_i} \tag{3}$$

where U^0 is the elastic strain energy of the shaft with crack and U^c is the additional strain energy due to the crack presence, as described by Eq. (4).

$$U^c = \int_{A_c} J(A_c) dA_c = \int_{A_c} \frac{1-\upsilon}{E} \left[\left(\sum_{i=1}^{6} K_{Ii} \right)^2 + \left(\sum_{i=1}^{6} K_{IIi} \right)^2 + (1+\upsilon) \left(\sum_{i=1}^{6} K_{IIIi} \right)^2 \right] dA_c \tag{4}$$

where $J(A_c)$ is the energy density function of deformation over the area of the shaft section with crack, E is the Young's modulus, ν is the Poisson's ratio, K_{Ii}, K_{IIi}, and K_{IIIi} are the stress intensity factors (SIF) associated with the crack load modes I, II, and III, respectively. In this case, only the crack load mode I is considered since the principal load is applied normal to the crack plane (Anderson, 2005). The additional flexibility c_{ij} is obtained as presented in Eq. (5).

$$c_{ij} = \frac{\partial^2 U^c}{\partial P_i \partial P_j} = \frac{\partial^2}{\partial P_i \partial P_j} \left[\int_{A_c} J\left(A_c\right) dA_c \right] \tag{5}$$

where the resulting integrals were obtained by using the procedure described in Papadopoulos (Papadopoulos, 2004).

Equation (6) shows the additional flexibility matrix due to the crack (**c**). This matrix is included in the flexibility matrix of the healthy shaft ($\mathbf{c_0}$) to obtain the resulting flexibility of the shaft FE with crack.

$$\mathbf{c_{ce}} = \mathbf{c_0} + \mathbf{c} \tag{6}$$

The Mayes' model suggests that a cosine function governs the opening and closing behavior of the crack. The crack is fully open when η coincides with the negative direction of Z ($180\,^\circ$ to the Z axis) and fully closed when η coincides with the positive direction of Z ($0\,^\circ$ or $360\,^\circ$ to the Z axis), as shown in Fig. 4.

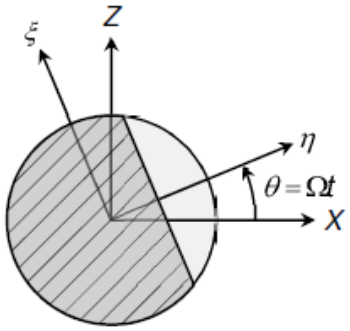

Figure 4. Rotating and fixed coordinates for the rotating shaft with a crack (θ represents the angular position of the crack and the dashed area represents the section of the shaft without crack).

The stiffness of the shaft with a crack in rotating coordinates ($\mathbf{k}_{RMayes}$ in a matrix representation) according to the Mayes' model is given by Eq. (7).

$$\mathbf{k}_{RMayes} = \begin{bmatrix} k_{\xi M}(\theta) & 0 \\ 0 & k_{\eta M}(\theta) \end{bmatrix} \tag{7}$$

where C_1 = cos(θ). For the angles $\theta = 0^\circ$ and $\theta = 360^\circ$ one has to $k_{\xi M}(0^\circ) = k_{\xi M}(360^\circ) = k_0$ and $k_{\eta M}(0^\circ) = k_{\eta M}(360^\circ) = k_0$ (stiffness of the shaft with the crack closed; equivalent to the shaft without crack). When the angle $\theta = 180^\circ$, $k_{\xi M}(180^\circ) = k_\xi$ and $k_{\eta M}(180^\circ) = k_\eta$, the crack remains fully open.

The stiffness k_ξ and k_η are obtained from the inverse of $\mathbf{c}_{ce}$ ($\mathbf{k}_{ce} = \mathbf{c}_{ce}^{-1}$; $k_\xi = k_{ce}(1,1)$ and $k_\eta = k_{ce}(2,2)$. Similarly, k_0 is obtained from the inverse of the flexibility matrix $\mathbf{c}_0$ ($\mathbf{k}_0 = \mathbf{c}_0^{-1}$; $k_0 = k_0(1,1) = k_0(2,2)$).

In fixed coordinates, the stiffness of the shaft with crack ($\mathbf{k}_{FMayes}$ in a matrix representation) is determined by applying the transformation given by Eq. (8).

$$\mathbf{k}_{FMayes} = \mathbf{T}^T \mathbf{k}_{RMayes} \mathbf{T} \tag{8}$$

$$\mathbf{T} = \begin{bmatrix} \cos(\theta) & \sin(\theta) \\ -\sin(\theta) & \cos(\theta) \end{bmatrix} \tag{9}$$

The stiffness matrices of the shaft FE with crack is obtained by combining the stiffness matrices presented above. Details on this procedure can be found in Cavalini Jr *et al.* (2016).

4. COMBINATION RESONANCES

Ishida and Yamamoto (2013) describes the conditions required for the appearance of resonances in the vibration responses of rotating machines. According to the authors, sub-harmonic, super-harmonic, and combination resonances can occur when the natural frequencies, rotation speed, and/or external excitation frequency have specific relationships.

In the vicinity of the rotation speed Ω, where Ω becomes an integer multiple of a natural frequency p_i ($\Omega \approx \pm m p_i$), a sub-harmonic resonance appears at $\Omega_i = \pm\Omega/m\,(\approx p_i)$. Differently, when $m\Omega\,(\approx p_i)$ holds, a super-harmonic resonance at $\Omega_i = \pm m\omega\,(\approx p_i)$ appears. In a rotor with multiple degrees of freedom with natural frequencies p_i, p_j, ..., where the relation $\Omega = \pm m p_i \pm n p_j \pm \cdots$ is present, the combination resonances $\Omega_i\,(\approx p_i)$ and $\Omega_j\,(\approx p_j)$ appear. Similarly, when an external force is applied in the rotating shaft at Ω, ω_i, ..., a combination resonance frequency at $\Omega = \pm m\Omega \pm n\omega_i \pm \cdots \approx p_i$ occurs (Ishida and Yamamoto, 2013).

Thus, combination resonances can be understood as the appearance of new peaks in the spectral responses of the rotor due to the nonlinear crack effect associated with the application of external forces (at frequency Ω_{diag}) and the shaft

rotation speed. The appearance of these new frequencies in the context of this work is associated with the presence of transverse cracks along the shaft.

The external force frequency Ω_{diag} can be obtained based on the multiple scales method, that determines the conditions required to create the combination resonances, as presented in Eq. (10) (Dohnal and Verhulst, 2008; Sawicki and Kulesza, 2015; Cavalini Jr *et al.*, 2016).

$$\Omega_{diag} = |n\Omega - \omega_{\Omega}| \tag{10}$$

where $n = \pm1, \pm2, \pm3, \ldots$, Ω is the rotation speed, and ω_{Ω} is a critical speed (forward whirl) of the rotor.

The multiple scales method is an asymptotic perturbation approach used for the solution of equations of motions associated with nonlinear systems (Sanches *et al.*, 2012). To illustrate the method, consider an undamped 1 DOF rotor with mass m, including a transversal crack and excited by two different frequencies Ω and Ω_{diag}. Equation (11) represents the behavior of this system. Note that the crack model influences the frequencies Ω and 2Ω.

$$\begin{aligned} m\ddot{q}(t) + \frac{1}{2}(k_0 + k_\xi)\, q(t) + \frac{1}{2}(k_0 + k_\xi)\cos(\Omega t)\, q(t) + ... \\ ... + \frac{1}{2}(k_0 + k_\xi)\cos(2\Omega t)\, q(t) = F\sin(\Omega t) + F_{diag}\sin(\Omega_{diag} t) \end{aligned} \tag{11}$$

Assuming that the stiffness change $(k_0 - k_\xi)$ is small as compared with the uncracked stiffness (k_0), it is possible introduce the parameter ε, as showed in Eq. (12).

$$\begin{aligned} \tfrac{1}{2}(k_0 - k_\xi) &= \varepsilon k_{D\xi} \\ \tfrac{1}{2}(k_0 + k_\xi) &= \varepsilon k_{M\xi} \end{aligned} \tag{12}$$

By using the method of multiple scales, it is valid to assume the expansion of Eq. (11) in a independent time scales $(T_j = \varepsilon^j t)$ (Nayfeh, 2000).

$$q(t,\varepsilon) = q_0(T_0, T_1, T_2, \ldots) + \varepsilon q_1(T_0, T_1, T_2, \ldots) + \varepsilon^2 q_2(T_0, T_1, T_2, \ldots) + \cdots \tag{13}$$

It is an important to highlight that the number of required independent time scales must be the same as the terms used in the expansion (Thomsen, 2013). By scaling the periodic terms to appear as parametric excitations at the first order of ε, Eq. (11) assume the form of Eqs. (14) and (15).

$$mD_0^2 q_0(T_0, T_1) + k_{M\xi} q_0(T_0, T_1) = F\sin(\Omega t) + F_{diag}\sin(\Omega_{diag} t) \tag{14}$$

$$\begin{aligned} mD_0^2 q_1(T_0, T_1) + k_{M\xi} q_1(T_0, T_1) + 2mD_1 D_0 q_0(T_0, T_1) + ... \\ ... + \frac{1}{2}k_{D\xi} q_0(T_0, T_1)\, e^{i\Omega T_0} + \frac{1}{2}k_{D\xi} q_0(T_0, T_1)\, e^{-i\Omega T_0} + ... \\ ... + \frac{1}{2}k_{D\xi} q_0(T_0, T_1)\, e^{2i\Omega T_0} + \frac{1}{2}k_{D\xi} q_0(T_0, T_1)\, e^{-2i\Omega T_0} \end{aligned} \tag{15}$$

where D_0 and D_1 are the partial derivative of a function with T_0 and T_1. The solution of Eq. (14) can be written as shown in Eq. (16).

$$\begin{aligned} q_0(T_0, T_1) = A_1(T_1)\, e^{i\omega_{0\xi} T_0} + \bar{A}_1(T_1)\, e^{-i\omega_{0\xi} T_0} + A_2(T_1)\, e^{i\Omega T_0} + \bar{A}_2(T_1)\, e^{-i\Omega T_0} + ... \\ ... + A_3(T_1)\, e^{i\Omega_{diag} T_0} + \bar{A}_3(T_1)\, e^{-i\Omega_{diag} T_0} \end{aligned} \tag{16}$$

where $\omega_{0\xi} = \left(\frac{k_{M\xi}}{m}\right)^{1/2}$, A_n, and its conjugate $\bar{A}_n$ are the amplitudes.

By substituting Eq. (16) into Eq. (15), the conditions necessary to induce the system to resonances arise, i.e, when $\omega_{0\xi} = \Omega \pm \Omega_{diag}$ and $\omega_{0\xi} = 2\Omega \pm \Omega_{diag}$, as given by Eq. (17). Only the combinations associated with Eq. (10) are shown in Eq. (17). The remaining terms were neglected. Other harmonic components as $cos(3\Omega t), cos(4\Omega t), \cdots$, would result in combinations like $3\Omega \pm \Omega_{diag}, 4\Omega \pm \Omega_{diag}, \cdots$.

$$\begin{aligned} mD_0^2 q_1(T_0, T_1) + k_{M\xi} q_1(T_0, T_1) = -... \\ ... - \bar{A}_3(T_1)\frac{1}{2}k_{D\xi} e^{iT_0(\Omega - \Omega_{diag})} - A_3(T_1)\frac{1}{2}k_{D\xi} e^{-iT_0(\Omega - \Omega_{diag})} - ... \\ ... - A_3(T_1)\frac{1}{2}k_{D\xi} e^{iT_0(\Omega + \Omega_{diag})} - \bar{A}_3(T_1)\frac{1}{2}k_{D\xi} e^{-iT_0(\Omega + \Omega_{diag})} - ... \\ ... - A_3(T_1)\frac{1}{2}k_{D\xi} e^{iT_0(2\Omega - \Omega_{diag})} - \bar{A}_3(T_1)\frac{1}{2}k_{D\xi} e^{-iT_0(2\Omega - \Omega_{diag})} - ... \\ ... - A_3(T_1)\frac{1}{2}k_{D\xi} e^{iT_0(2\Omega + \Omega_{diag})} - \bar{A}_3(T_1)\frac{1}{2}k_{D\xi} e^{-iT_0(2\Omega + \Omega_{diag})} \end{aligned} \tag{17}$$

5. NUMERICAL AND EXPERIMENTAL RESULTS

Table (2) presents the excitation frequencies of the external force $\mathbf{F_{diag}}$ determined using the first forward whirl critical speed (53.09 Hz) and the rotation speed $\Omega = 1200$ rev/min, as given by Eq. (10).

Table 2. Excitation frequencies of the external force $\mathbf{F_{diag}}$.

n	Excitation frequency [Hz]	n	Excitation frequency [Hz]
-1	73.09	+1	33.09
-2	93.09	+2	13.09
-3	113.09	+3	6.91
-4	133.09	+4	26.01
-5	153.09	+5	46.91

Figure 5 shows the simulated vibration responses of the healthy and faulty rotor FE model (sensor S_{8X}). A crack located at the element #22 with 10%, 20%, 30%, 40%, and 50% depths (applied separately) was considered as the faulty condition. The crack position is in agreement with the fault introduced in the experimental test-rig (see Fig. 1). A residual unbalance condition was considered to obtain these results. In this case, an external force of 25 N amplitude and 73.09 Hz frequency ($\mathbf{F_{diag}}$) was applied along the horizontal direction of the bearing B_2 in the FE model (the position corresponding to the node #32). The vibration responses of the rotor FE model without the application of the external force are also presented for comparison purposes.

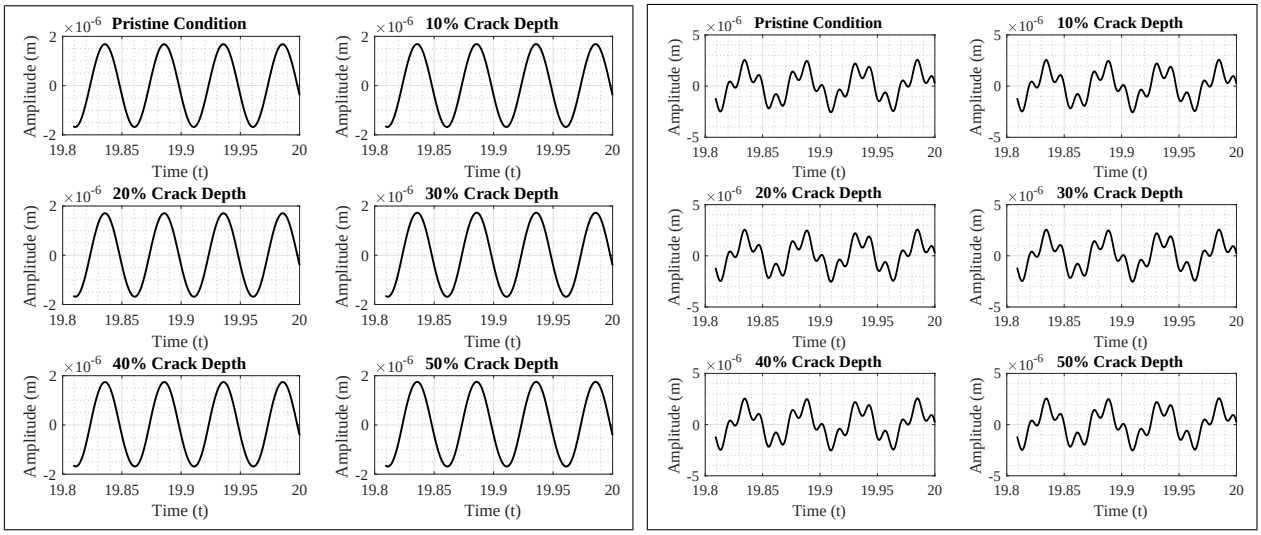

(a) External excitation absent (b) External exitation present

Figure 5. Time domain vibration responses of the system for different shaft conditions - Sensor S_{8X}.

Figure 6 presents the orbits determined using the sensors S_{8X} and S_{8Z} (orbits corresponding to the vibration responses shown in Fig. 5). In this case, a particular shape is observed in the orbits due to the crack and external excitation presences.

Figure 7 shows the spectral responses of the healthy and faulty rotor FE model as given by Fig. 5a, i.e., without the application of the external force. The vibration responses obtained applying the external excitation are presented in Fig. 8 (time domain vibration responses presented in Fig. 5b). Figure 9 shows the corresponding experimental results obtained for a 50% crack depth.

As expected, the combination resonances appear only when the external force is applied. Only the harmonic components due to the crack presence are observed in Fig. 8. Additionally, Fig. 8 demonstrates that the amplitude of the peaks at the combination resonances changes according to the crack severity. Finally, similar numerical and experimental results were obtained when the external force was applied (see Fig. 8 and 9).

6. FINAL REMARKS

This work was dedicated to present the combination resonance approach as a possible technique for crack detection in rotating machines. The crack presence in the shaft introduces additional flexibility, which was determined in the present contribution using the strain energy density criterion and the linear fracture mechanics theory. The breathing behavior of

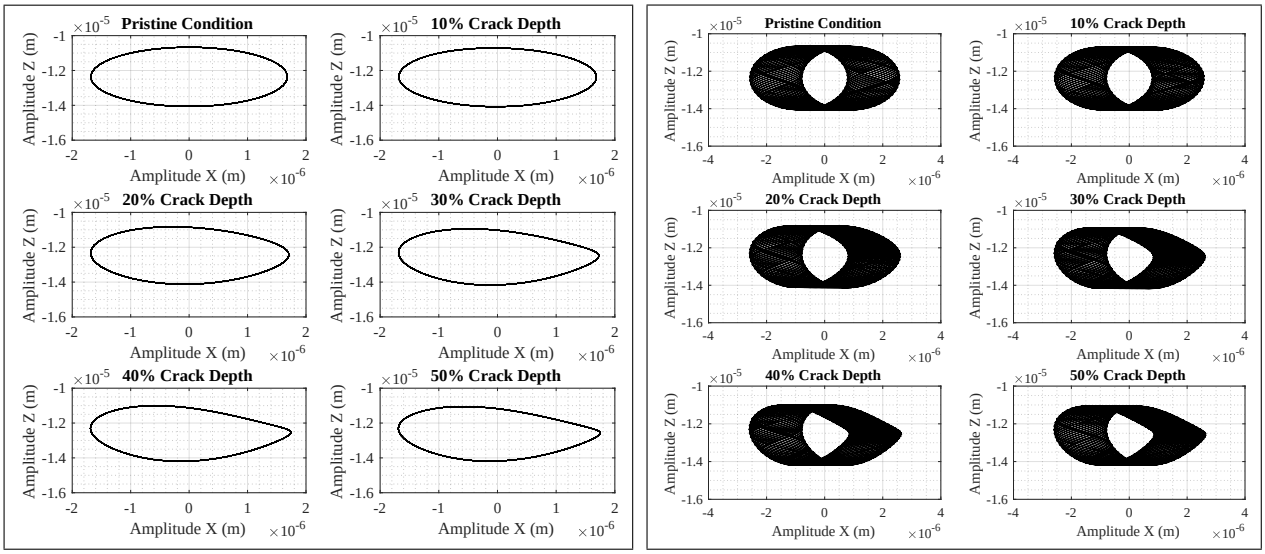

(a) External excitation absent (b) External excitation present

Figure 6. Shaft orbits for different shaft conditions - Sensors S_{8X} and S_{8Z}.

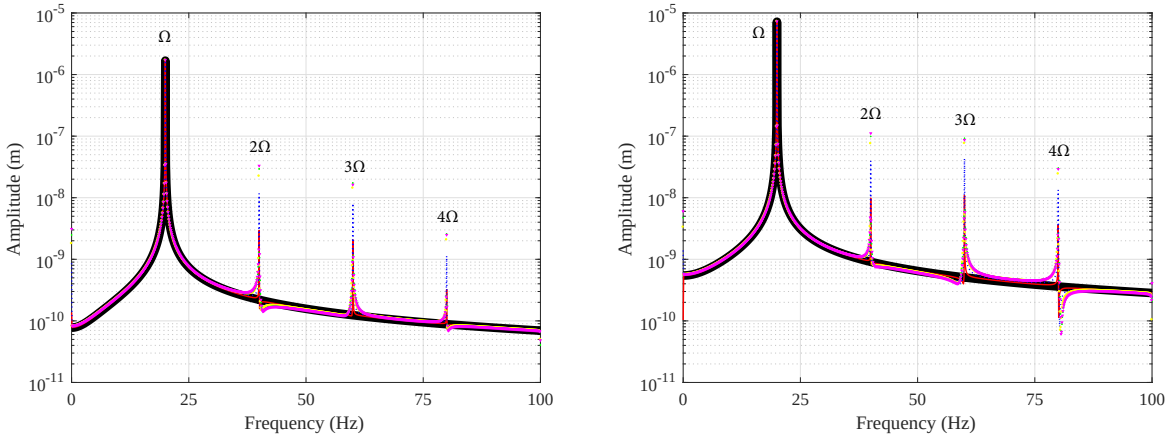

(a) Position S_{8X} (b) Position S_{28X}

Figure 7. DFTs obtained without external force. — Pristine Condition; — 10% crack depth; ··· 20% crack depth; ○ 30% crack depth; × 40% crack depth; ▽ 50% crack depth.

the crack was modeled according to the Mayes' model. In this context, the effects of a transverse crack in the vibration responses of a rotor test-rig were evaluated. An external force was applied to induce combination resonances in the vibration responses of the considered rotating shaft with crack. The numerical and experimental results demonstrated to be similar. Further research effort will be dedicated to improving and obtained more experimental results.

7. ACKNOWLEDGMENTS

The authors are thankful for the financial support provided to the present research effort by CNPq (574001/2008-5,304546/2018-8, and 431337/2018-7), FAPEMIG (TEC-APQ-3076-09, TEC-APQ-02284-15, TEC-APQ-00464-16, and PPM-00187-18), and CAPES through the INCT-EIE.

8. REFERENCES

Anderson, T.L., 2005. *Fracture mechanics: fundamentals and applications*. CRC press.

Bachschmid, N., Pennacchi, P. and Tanzi, E., 2010. *Cracked rotors: a survey on static and dynamic behaviour including modelling and diagnosis*. Springer Science & Business Media.

Cavalini Jr, A.A., Sanches, L., Bachschmid, N. and Steffen Jr, V., 2016. "Crack identification for rotating machines based on a nonlinear approach". *Mechanical Systems and Signal Processing*, Vol. 79, pp. 72–85.

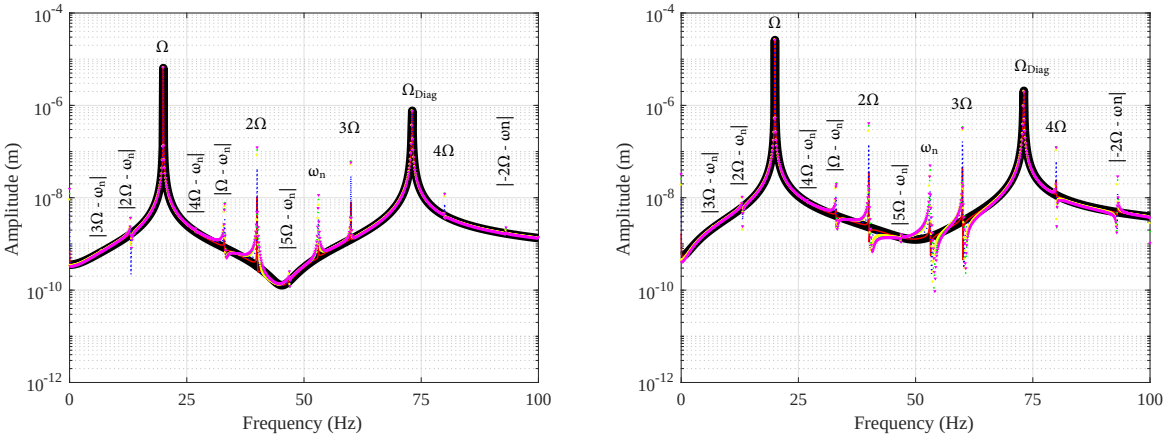

(a) Position S_{8X} (b) Position S_{28X}

Figure 8. DFTs obtained by using the external force frequency Ω_{diag} = 73.09 Hz. — Pristine Condition; — 10% crack depth; ··· 20% crack depth; ○ 30% crack depth; × 40% crack depth; ▽ 50% crack depth.

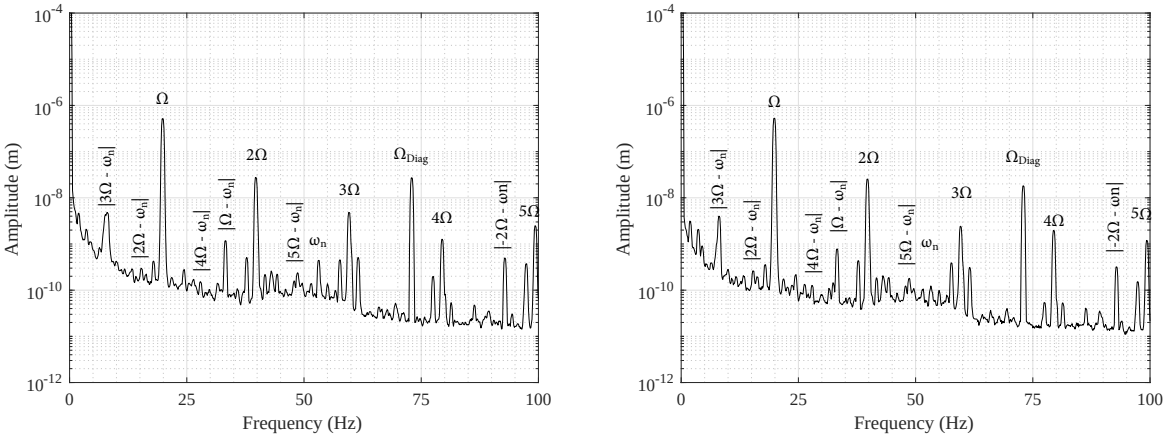

(a) Position S_{8X} (b) Position S_{28X}

Figure 9. Experimental DFTs obtained by using the external force frequency Ω_{diag} = 73.09 Hz with 50% crack depth.

Darpe, A.K., Gupta, K. and Chawla, A., 2004. "Coupled bending, longitudinal and torsional vibrations of a cracked rotor". *Journal of sound and vibration*, Vol. 269, No. 1-2, pp. 33–60.

Dohnal, F. and Verhulst, F., 2008. "Averaging in vibration suppression by parametric stiffness excitation". *Nonlinear Dynamics*, Vol. 54, No. 3, pp. 231–248.

Gasch, R., 1976. "Dynamic behaviour of a simple rotor with a cross-sectional crack". In *Proc. Int. Mech. Eng. Conf.* Vol. 123.

Grabowski, B., 1980. "The vibrational behavior of a turbine rotor containing a transverse crack". *Journal of Mechanical Design*, Vol. 102, No. 1, pp. 140–146.

Ishida, Y. and Yamamoto, T., 2013. *Linear And Nonlinear Rotordynamics: a modern treatment with applications*. John Wiley & Sons.

Iwatsubo, T., Arii, S. and Oks, A., 1992. "Detection of a transverse crack in a rotor shaft by adding external force". In *Institution of Mechanical Engineers Conference Publications*. MEDICAL ENGINEERING PUBLICATIONS LTD, Vol. 6, pp. 275–275.

Lu, Z., Dong, D., Ouyang, H., Cao, S. and Hua, C., 2017. "Localization of breathing cracks in stepped rotors using super-harmonic characteristic deflection shapes based on singular value decomposition in frequency domain". *Fatigue & Fracture of Engineering Materials & Structures*, Vol. 40, No. 11, pp. 1825–1837.

Mayes, I.W. and Davies, W.G.R., 1984. "Analysis of the response of a multi-rotor-bearing system containing a transverse crack in a rotor". *Journal of vibration, acoustics, stress, and reliability in design*, Vol. 106, No. 1, pp. 139–145.

Nayfeh, A.H., 2000. *Nonlinear interactions: analytical, computational, and experimental methods*. Wiley New York.

Papadopoulos, C., 2004. "Some comments on the calculation of the local flexibility of cracked shafts". *Journal of Sound*

and Vibration, Vol. 4, No. 278, pp. 1205–1211.

Saavedra, P. and Cuitino, L., 2002. "Vibration analysis of rotor for crack identification". *Modal Analysis*, Vol. 8, No. 1, pp. 51–67.

Sanches, L., Michon, G., Berlioz, A. and Alazard, D., 2012. "Parametrically excited helicopter ground resonance dynamics with high blade asymmetries". *Journal of Sound and Vibration*, Vol. 331, No. 16, pp. 3897–3913.

Sawicki, J.T. and Kulesza, Z., 2015. "Stability of a cracked rotor subjected to parametric excitation". *Journal of Engineering for Gas Turbines and Power*, Vol. 137, No. 5, p. 052508.

Sawicki, J.T., Sen, A.K. and Litak, G., 2009. "Multiresolution wavelet analysis of the dynamics of a cracked rotor". *International Journal of Rotating Machinery*, Vol. 2009.

Sinou, J.J. and Lees, A., 2005. "The influence of cracks in rotating shafts". *Journal of sound and vibration*, Vol. 285, No. 4-5, pp. 1015–1037.

Storn, R. and Price, K., 1995. "Differential evolution-a simple and efficient adaptive scheme for global optimization over continuous spaces [r]". *Berkeley: ICSI*.

Thomsen, J.J., 2013. *Vibrations and stability: advanced theory, analysis, and tools*. Springer Science & Business Media.

Zhao, J., DeSmidt, H. and Yao, W., 2014. "Nonlinear dynamics of breathing cracked jeffcott rotor under axial excitation". In *ASME 2014 Dynamic Systems and Control Conference*. American Society of Mechanical Engineers, pp. V001T08A003–V001T08A003.